Light confinement via periodic modulation of the refractive index

A Alberucci[1,4], L Marrucci[2,3] and G Assanto[1]

[1] Nonlinear Optics and OptoElectronics Laboratory, University Roma Tre, Via della Vasca Navale 84, I-00146 Rome, Italy
[2] Dipartimento di Fisica, Università di Napoli Federico II, Napoli, Italy
[3] CNR-SPIN, Complesso Universitario di Monte Sant'Angelo, Napoli, Italy
E-mail: alessandro.alberucci@gmail.com

Abstract. We investigate, both theoretically and numerically, light confinement in dielectric structures with a transverse refractive index distribution periodically modulated in the longitudinal coordinate. We demonstrate that light can be guided even in the balanced limit when the average refractive index contrast vanishes in the direction of propagation, a dynamic trapping phenomenon analogous to the Kapitza effect in quantum mechanics. Finally, with reference to segmented waveguides with an unbalanced index modulation, we address the interplay of dynamic and static confinements.

[4] Author to whom any correspondence should be addressed.

Contents

1. Introduction

Periodic structures are essential in photonics, as they support various phenomena that are useful in controlling and managing light signals and beams. The periodic modulation of the refractive index in the propagation direction allows the realization of, for instance, filters and coatings, diffractive and coupling gratings, distributed feedback reflectors and resonators, and quasi-phase matching for parametric generation [1–5]. An index periodicity in the transverse plane is at the basis of waveguide arrays for discrete diffraction [6]; periodic arrangements in two or three dimensions entail the realization of photonic crystals [7].

In this paper, we focus on refractive index structures featuring a bell-shaped profile in the transverse plane and periodically modulated along the direction z of light propagation. A longitudinal modulation on light propagation was previously addressed in the case of waveguide arrays with reference to the linear refractive index [8] and the nonlinearity [9, 10]; experiments were reported on nonlinear inhibition of tunneling [11] as well as on quasi-Bloch oscillations [12]. Regarding single-waveguide structures, similar geometries were studied in the context of segmented waveguides, that is, light-confining sections alternating along z with transversely homogeneous portions where light could diffract [2, 13–16]. It was demonstrated that, in most cases, segmented waveguides can be modeled and operate as continuous waveguides with a transverse index profile given by the spatial averaging along the modulated direction z [17].

The aim of the work hereby is to extend and generalize the treatment of z-periodic optical waveguides to those with a zero mean longitudinal modulation, that is, an index modulation of alternating signs along $\hat{z}$. In the case of zero mean contrast, one would intuitively expect light to diffract owing to the alternation of index wells (focusing regions) and of index barriers (defocusing regions) of finite transverse extent. However, in the context of quantum mechanics, it is understood that the fast-scale particle motion driven by a rapidly

oscillating potential (in time) gives rise to an additional time-independent effective potential that can, in turn, induce a slow-scale dynamics of the particle [18]. This effect, known as the Kapitza effect from the original work of the Russian Nobel laureate on a mechanic pendulum [19], was exploited by the Nobel laureate Paul [20] to realize particle traps. Since paraxial light propagation in the harmonic regime and the motion of quantum particles are both governed by the Schrödinger equation with the spatial coordinate z taking the role of an equivalent time [21], the analogy between optical propagation and the Kapitza effect in quantum mechanics suggests the insurgence of an effective refractive index distribution even in zero-mean-contrast periodically segmented waveguides, a distribution uniform along z and possibly able to transversely trap light. If an oscillating potential in quantum mechanics gives rise to a steady effective potential proportional to the square of the gradient of the periodic modulation [18, 22], in optics a bell-shaped transverse distribution of a z periodic refractive index results in a double-humped trapping well. Optical analogies of the Kapitza effect have been theoretically discussed, limited to waveguide arrays [23] or transversely invariant dielectric stacks [24]. In the first case, discrete diffraction is inhibited by a longitudinal modulation of the coupling strength between standard waveguides [23]. In the second, a (rather large) periodic modulation of the dielectric susceptibility can suppress diffraction of transverse-magnetic waves by minimizing the longitudinal field component [24]. At variance with these previous reports, the approach we discuss here entails light trapping solely via a photonic equivalent of the Kapitza effect: wave confinement is polarization independent and scales fully with wavelength.

We consider transversely limited (waveguide-like) index structures periodically modulated and balanced along z, i.e. with a vanishing mean index contrast in the propagation direction. Initially we treat the problem analytically and later verify our theoretical results using the beam propagation method (BPM), the latter also allowing us to assess the validity of the effective potential approximation. Finally, we extend our study to unbalanced periodic waveguides with a nonzero mean index contrast, addressing the interplay between *static* confinement due to the average distribution (bell shaped in the transverse plane) and *dynamic* Kapitza-like confinement stemming from the modulation.

2. Theoretical background

For the sake of simplicity we refer to planar guided-wave structures, i.e. (1+1)D geometries. Under the paraxial approximation, lightwave propagation is governed by the Schrödinger-like equation

$$2ik_0 n_0 \frac{\partial A}{\partial z} + \frac{\partial^2 A}{\partial x^2} + 2n_0 k_0^2 \Delta n(x, z) A = 0, \tag{1}$$

where A is the field envelope, n_0 is the unperturbed refractive index, k_0 is the vacuum wavenumber and Δn is the index profile in the transverse space, i.e. along x. The use of equation (1) to describe light dynamics implies discarding the back-reflected wave components (i.e. propagating along $-\hat{z}$), always present in a periodic structure owing to longitudinal index variations. Such approximation is usually valid unless Bragg resonances occur [13].

We take the index well to be factorizable, i.e. $\Delta n(x, z) = f(z)U(x)$ and the ansatz

$$A(x, z) = \phi(x, z) e^{ik_0 U(x) \int_{z_0}^{z} f(z') \, dz'}. \tag{2}$$

We normalize to unity the maximum absolute value of $f(z)$. By substituting equation (2) into equation (1) we obtain [18]

$$2ik_0 n_0 \frac{\partial \phi}{\partial z} + \frac{\partial^2 \phi}{\partial x^2} + 2ik_0 \, g(z) \left(\frac{\partial U}{\partial x} \frac{\partial \phi}{\partial x} + \frac{1}{2} \frac{\partial^2 U}{\partial x^2} \phi \right) - k_0^2 \, g^2(z) \left(\frac{\partial U}{\partial x} \right)^2 \phi = 0, \tag{3}$$

where we introduce $g(z) = \int_{z_0}^z f(z') \, dz'$. By dealing with a periodic $f(z) = f(z + \Lambda)$, we can expand it in a Fourier series, $f(z) = \sum_{l=-\infty}^{\infty} f_l \exp(2\pi i l z / \Lambda)$. We assume $\overline{f} = \frac{1}{\Lambda} \int_0^\Lambda f(z) \, dz = f_0 = 0$, i.e. $f(z)$ with a zero mean. It is straightforward to get $g(z) = G(z) - G(z_0)$, where $G(z) = \frac{\Lambda}{2\pi i} \sum_{l=-\infty}^{\infty} \frac{f_l}{l} \exp(2\pi i l z / \Lambda)$. We note that $\overline{g} = 0$ only if $G(z_0) = 0$. Applying the Fourier transform operator to equation (3), since the spectra of both $g(z)$ and its square $g^2(z)$ consist of series of Dirac functions, equation (3) relates the spectrum $\tilde{\phi}(\beta) = \int \phi \exp(i\beta z) \, dz$ to its replicas centered in $\beta_m = 2\pi m / \Lambda$ ($m \in \mathbb{Z}$). If the width $\Delta\beta$ of $\tilde{\phi}$ is smaller than β_1, sideband copies of $\tilde{\phi}$ do not interact with the baseband (more precisely their overlap is negligible because $\tilde{\phi}$ is necessarily nonzero for all the spatial frequencies β). To derive a quantitative condition, we choose a bell-shaped profile for field ϕ. After approximating the wavefunction with a Gaussian of waist w_0, the anti-aliasing condition reads

$$w_0 > \frac{\Lambda}{\pi}. \tag{4}$$

Equation (4) can be intuitively interpreted in terms of alternating focusing/defocusing regions: narrow wavepackets (beams) undergo strong spreading when $f(z) < 0$; when light reaches the next focusing region along z, the beam width is too large and lensing is insufficient to trap and confine the field. When equation (4) is satisfied, the application of the extra condition $\overline{g} = 0$ to equation (3) yields

$$2ik_0 n_0 \frac{\partial \phi}{\partial z} + \frac{\partial^2 \phi}{\partial x^2} - k_0^2 \overline{g^2(z)} \left(\frac{\partial U}{\partial x} \right)^2 \phi = 0. \tag{5}$$

The term $-\overline{g^2(z)} \left(\frac{\partial U}{\partial x} \right)^2$ plays the role of an effective index difference Δn_{eff}. The condition $\overline{g} = 0$, easily satisfied by a proper choice of z_0, is required to zero the contribution from the third term in equation (3) (the role of the initial phase of the potential is well addressed in [25]). In physical terms, we expect that the *quasi-modes* of equation (1), if they exist, feature phase fronts with a periodically varying curvature (see equation (2)), as determined by the focusing or defocusing character of the local index profile [17]. Equation (5) predicts that an effective index distribution

$$\Delta n_{\text{eff}} = -\frac{\Lambda^2}{4\pi^2} \left(\sum_{l=-\infty}^{\infty} \frac{f_l f_{-l}}{l^2} \right) \left(\frac{\partial U}{\partial x} \right)^2 \tag{6}$$

acts on the wavepacket. According to equation (6) the effective photonic potential is proportional to the square of the modulation period Λ. Thus, for short Λ, the longitudinal index variations are too fast and light is not affected by the modulation. When Λ gets longer the dynamic effects increase indefinitely, clearly an unphysical result: in fact, equation (6) is valid only if condition (4) is satisfied. Summarizing, we expect dynamic (Kapitza-like) trapping to be maximum for a finite value of the modulation period Λ_{max}.
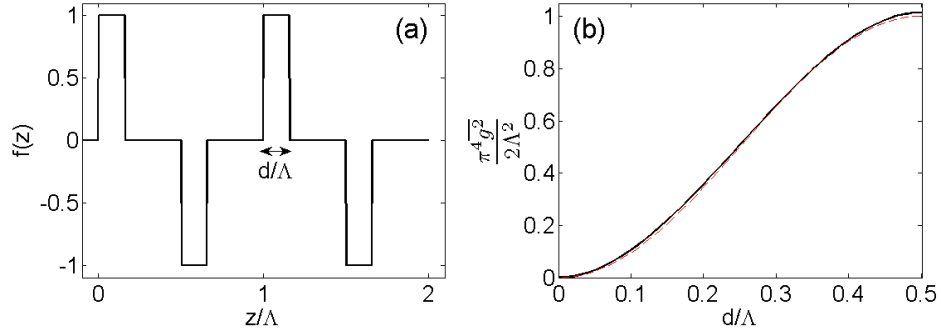
Figure 1. (a) Plot of $f(z)$ versus the normalized propagation coordinate z/Λ for a flat-top modulation. (b) Behavior of $\overline{g^2}$ (given by equation (8)) for $f(z)$ as plotted in (a) versus d/Λ; solid and dashed lines correspond to the series computed up to $l = 50$ and 1, respectively.

2.1. Dependence of the photonic Kapitza effect on the modulation profile

Equation (6) states the dependence of the effective potential Δn_{eff} on the longitudinal modulation $f(z)$ via the Fourier coefficients f_l. To address such dependence, we first consider the simplest case of a sinusoidal modulation $f(z)$. Equation (6) yields

$$\overline{g^2} = \frac{\Lambda^2}{8\pi^2},\tag{7}$$

and it is also $z_0 = \Lambda/4$ in order to ensure $G(z_0) = 0$. Next, we consider a flat-top modulation, featuring two segments of length d with opposite amplitudes per period (see figure 1(a)). We obtain

$$\overline{g^2} = \frac{2\Lambda^2}{\pi^4} \sum_{l=1}^{\infty} \frac{1}{l^4} \sin^2\left(\frac{\pi l}{2}\right) \sin^2\left(\frac{\pi l d}{\Lambda}\right).\tag{8}$$

When $d = \Lambda/2$, the modulating function $f(z)$ is a square wave; then equation (8) becomes $\overline{g^2} = \left(2\Lambda^2/\pi^4\right) \sum_{m=0}^{\infty} 1/(2m+1)^4$. The behavior of $\overline{g^2}$ is plotted in figure 1. The last step is finding out how the initial section z_0 depends on d and Λ. By setting $G(z_0 = 0)$ we get

$$z_0 = \frac{\Lambda - d}{2} + m\frac{\Lambda}{2} \quad (m \in \mathbb{Z}).\tag{9}$$

2.2. Physics of the effective index profile

The appearance of the effective index contrast Δn_{eff} can be physically understood from the superposition principle, in analogy to classical confinement being explained as a transverse phase modulation due to an inhomogeneous refractive index. Taking the ansatz

$$A = c \, e^{ik(z)x} \, e^{i \int_0^z E \, dz'}\tag{10}$$

with c an arbitrary constant, expanding Δn in a power series truncated to the linear term (i.e. $\Delta n(x, z) = \Delta n_0(z) + \Delta n_1(z)x$), and substituting (10) into equation (1) we get

$$k(z) = k_0 \int_0^z \Delta n_1(z') \, dz',\tag{11}$$

$$E(z) = \frac{k^2(z)}{2k_0 n_0} - k_0 \Delta n_0(z), \tag{12}$$

where we choose $k(0) = 0$ in equation (11). Owing to the periodicity of $\Delta n(z)$, the field A will be periodic as well; thus we can set $A(\Lambda) = A(0)\, e^{i\varphi}$. The phase difference φ accounts for the Kapitza effect acting on the wavepacket. The solution of equations (11) and (12) and its substitution in equation (10) provide

$$\varphi = \int_0^\Lambda E\, \mathrm{d}z' = \int_0^\Lambda \left(\frac{k^2(z')}{2k_0 n_0} - k_0 \Delta n_0(z') \right) \mathrm{d}z'. \tag{13}$$

The integral of Δn_0 vanishes due to the assumption of a zero mean for $f(z)$. Conversely, the integral along z of the *equivalent* kinetic energy $k^2/(2k_0 n_0)$ is nonzero, as the light momentum k is periodically modulated by the local index gradient $\Delta n_1 = f(t)\partial U/\partial x$. Summarizing, for the phase delay φ over a single period we find the expression

$$\varphi = \frac{k_0}{2n_0} \left(\frac{\partial U}{\partial x} \right)^2 \int_0^\Lambda g^2(z)\, \mathrm{d}z. \tag{14}$$

Equation (14) predicts the same effective index profile of equation (5). We conclude that the Kapitza effect is due to the longitudinal modulation of the equivalent kinetic energy induced by the periodicity [26]; for well-chosen transverse profiles $U(x)$, the transverse phase modulation can compensate diffraction. Noteworthy, in obtaining equation (14) we consider a periodic A, the latter assumption clearly invalid for long modulation periods as diffraction can induce appreciable changes in wave amplitude, consistently with condition (4).

3. Quasi-modes

In this section, we want to examine those cases in which the effective potential can support light trapping. The easiest configuration corresponds to bell-shaped $U(x)$: for instance, we can take super-Gaussian functions $U(x) = U_0 \exp\left(-x^{2p}/w_U^{2p}\right)$ ($p \in \mathbb{N}$). In this case, the effective index Δn_{eff} takes an inverted W-like transverse profile

$$\Delta n_{\mathrm{eff}} = -\frac{\Lambda^2 p^2 U_0^2}{\pi^2} \left(\sum_{l=-\infty}^{\infty} \frac{f_l f_{-l}}{l^2} \right) \frac{x^{2(2p-1)}}{w_U^{4p}} \exp\left(-\frac{2x^{2p}}{w_U^{2p}} \right). \tag{15}$$

The effective refractive index profiles Δn_{eff} are drawn in figure 2 for three values of the parameter p; for large p the super-Gaussian tends to a buried slab-like waveguide. As is well known, this structure does not support guided modes because the evanescent profiles at $|x| \to \infty$ lead to a leaky behavior even in the central lobe of the guide [27]. Such types of geometries in optics support leaky quasi-modes (corresponding to metastable states in quantum mechanics), actually consisting of a superposition of diffractive (free) modes [27].

We can compute the quasi-modes of the structure by using an index profile with the central lobe only, i.e. retaining the index distribution between the two local minima (see figure 2(b)); on the external regions we set the effective index to its global minimum. This approach works until the overlap of the calculated mode with the external portions of the effective index well can be neglected.
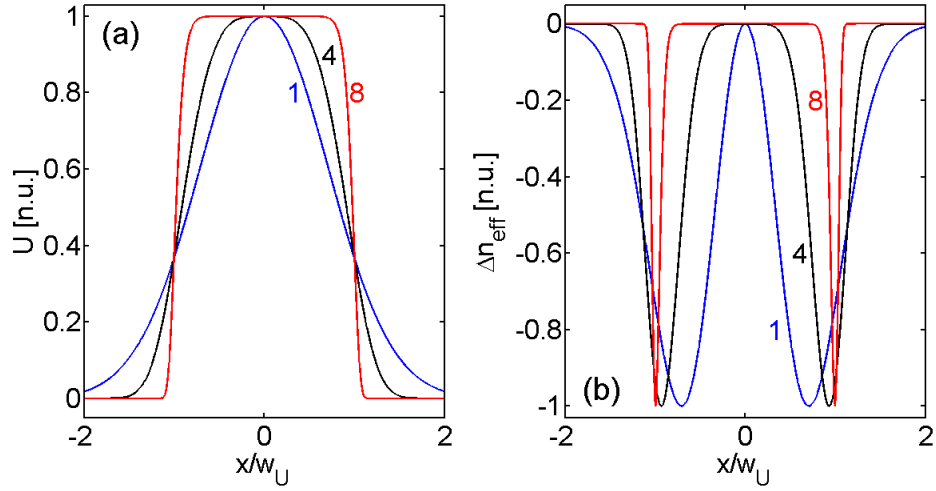
Figure 2. (a) Profile of $U(x)$ versus x and (b) corresponding effective refractive index contrast Δn_{eff}; we normalized the quantities to their maximum absolute value. The different lines in each panel correspond to $p = 1$ (blue), $p = 4$ (black) and $p = 8$ (red), respectively.

3.1. Gaussian trap

Let us take $p = 1$ in equation (15) and a sinusoidal oscillation for $f(z)$. In this case, the eigenvalue problem stemming from equation (5) can be scaled with respect to the normalized coordinate $x' = x/w_U$. Taking the ansatz $\phi(x, z) = u(x) \exp(i\Delta\beta_{\text{eff}}z)$, equation (5) provides

$$2k_0 n_0 w_U^2 \Delta\beta_{\text{eff}} u = \frac{\partial^2 u}{\partial x'^2} - \frac{k_0^2 \Lambda^2 U_0^2}{2\pi^2} F(x')u, \tag{16}$$

where $F(x') = x'^2 e^{-2x'^2} \text{rect}\left[x'/(2x_{\text{m}})\right] + \left[H(x' - x_{\text{m}}) + H(-(x' + x_{\text{m}}))\right] x_{\text{m}}^2 e^{-2x_{\text{m}}^2}$, with x_{m} the position of the local minimum of Δn_{eff} for positive x' and H the Heaviside step function.

According to equation (16), in the normalized reference system the shape of the mode does not depend on the width w_U of the index profile, if $U(x)$ is Gaussian; moreover, the effective index variation $\Delta N_{\text{eff}} = \Delta\beta_{\text{eff}}/k_0$ depends quadratically on w_U.

The modal profiles computed via a standard numerical procedure are plotted in figure 3. As predicted, the larger the modulation period Λ, the stronger the transverse confinement. At the same time, light trapping via the Kapitza effect improves as the depth of the index well U_0 increases; unlike in conventional waveguides, the trapping strength is proportional to the square of U_0. The trend of ΔN_{eff} versus Λ is graphed in figure 4(a). Firstly, we note that ΔN_{eff} is negative, corresponding to a propagation constant for mode u that is lower than $n_0 k_0$. Secondly, ΔN_{eff} decreases as Λ grows, i.e. as confinement gets stronger. The sign and the trend of ΔN_{eff} are opposite to the case of static confinement, in both continuous and segmented waveguides. Finally, the absolute value of ΔN_{eff} becomes larger as U_0 increases. Figure 4(b) shows the modal width $w_{\text{mode}} = 2\sqrt{\int x^2 |\phi|^2 \, \mathrm{d}x / \int |\phi|^2 \, \mathrm{d}x}$ versus Λ. For short periods the transverse size goes to infinity due to the absence of a trapping potential, whereas for large Λ the width tends to the diffraction-limited value λ. Equation (16) shows that the focusing strength depends on the product $U_0\Lambda$, as confirmed by the numerical results in figures 3 and 4.
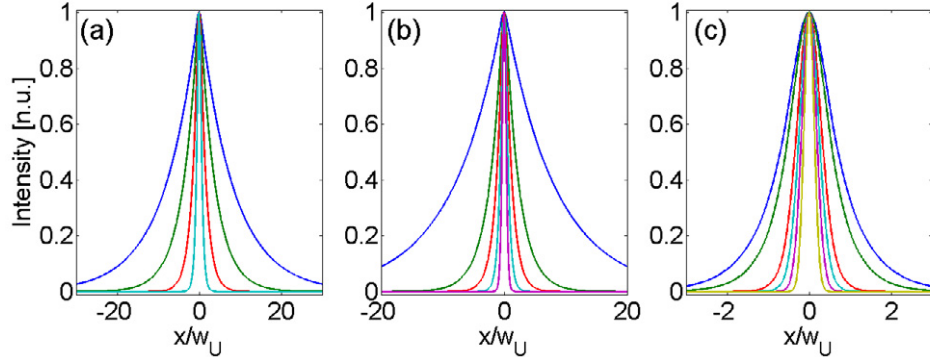
Figure 3. Numerically computed fundamental quasi-modes for $p = 1$ versus x/w_U when (a) $U_0 = 0.05$, (b) 0.1 and (c) 0.5, respectively. The curves correspond to period $\Lambda = 100, 50, 30, 20, 10$ and $8\,\mu$m from the narrowest to the largest profile; in panels (a) and (b) the results for $\Lambda = 8$ and 8, 10 μm respectively, are not shown as they are larger than 130, the size of our numerical window in normalized units. Here $\lambda = 1\,\mu$m.
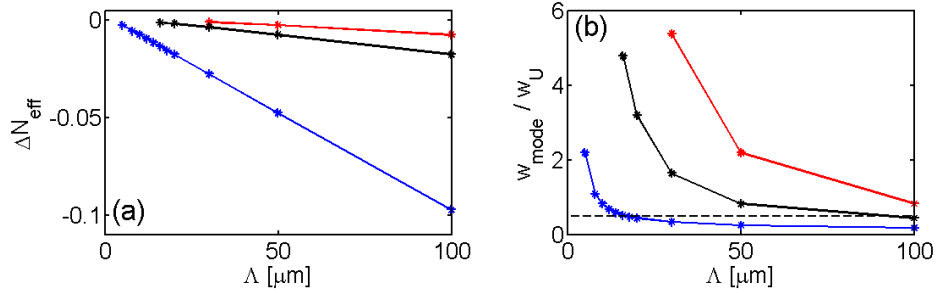
Figure 4. (a) ΔN_{eff} versus Λ and (b) width of the fundamental mode normalized to w_U for $U_0 = 0.5$ (blue line), $U_0 = 0.1$ (black line) and $U_0 = 0.05$ (red lines); in (a) and (b) the well depth decreases from the bottom to top curves. The dashed line in (b) represents $w_{\text{mode}} = w_u/2$. Here $\lambda = 1\,\mu$m.

The solutions in figure 3 are calculated neglecting the effects of the lateral lobes shown in figure 2(b). The mode of a W-shaped guide, however, is inherently leaky; thus we need to evaluate power losses of the wavepackets in figure 3 as they propagate. To this extent, we introduce the loss coefficient α via $\phi(x = 0, z) = \phi(x = 0, z = 0) \exp(-\alpha z)$ and define the attenuation length L_{damp} of the quasi-mode as $1/\alpha$ [27]. From the governing equation (5), we define a propagation length $z_{\text{norm}} = z/w_U^2$, similar to the normalization employed in the eigenvalue problem (16). Otherwise stated, if $L_{\text{damp}} = L_1$ for $w_U = w_1$, then it is $L_2 = (w_2/w_1)^2 L_1$ for w_2. Noteworthy, the damping length L_{damp} depends quadratically on the waist (approximately equal to w_U in the limit of strong confinement), in analogy to the Rayleigh distance; hence, the ratio between the diffractive losses due to a periodic index profile and those due to standard diffraction is constant: in the effective potential approximation the waveguiding does not depend on the width w_U of the index trap. L_{damp} can be numerically calculated with a BPM algorithm, accounting for the whole index landscape. Specifically, we consider at the
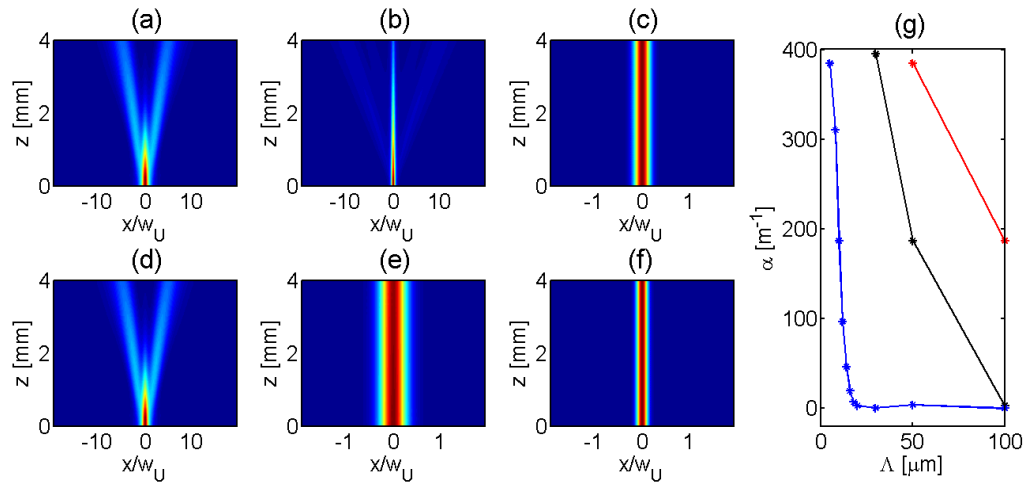
Figure 5. BPM computation of light propagation in the plane $(x/w_U, z)$ when the input field is the eigenmode computed from equation (16); the medium is assumed to be z-invariant with an effective index profile Δn_{eff}. The waveguide parameters in the top panels are $U_0 = 0.05$ (a), 0.1 (b) and 0.5 (c), with $\Lambda = 50\,\mu m$ in all of them; at the bottom $\Lambda = 5$ (d), 20 (e) and $100\,\mu m$ (f), with $U_0 = 0.5$ fixed. (g) Loss coefficient α versus Λ, each line corresponding to the data plotted in figure 4(b). Here $\lambda = 1\,\mu m$ and $w_U = 10\,\mu m$.

input the mode obtained from equation (16); then we solve equation (5) versus z and estimate the mode attenuation.

The results are shown in figure 5: as expected, the diffraction losses diminish when the depth U_0 of the index well (panels (a)–(c)) or the period Λ increase (panels (d)–(f)). Figure 5(g) summarizes the results by graphing α versus Λ. We note that the same α is obtained for different U_0 if the product ΛU_0 is conserved, as discussed above; thus, the curve for $U_0 = 0.1$ assumes a general character. A sharp transition is observed in α when $w_{\mathrm{mode}} \approx w_U/2$, i.e. the quasi-mode computed via equation (16) extends beyond the central lobe, in turn forcing non-negligible coupling to the radiation modes with larger transverse wavevector. This means that our approach is valid for $w_{\mathrm{mode}} < w_U/2$, that is, the region below the dashed line in figure 4(b). This condition does not yet guarantee light confinement, since equation (4) has not been accounted for. We deal with it in the next section.

4. Numerical results

Hereby we solve the full equation (1) in order to check the validity of the effective equation (5) for dynamic light trapping, verifying condition (4).

We consider the propagation of the quasi-modes in figure 3 for a fixed U_0 while varying the trap width w_U, i.e. we take quasi-modes belonging to the existence curves in figure 4(b). We first consider the quasi-modes (top line in figure 4(b)) not satisfying the condition $w_{\mathrm{mode}} < w_U/2$ and thus undergoing large diffraction losses, consistently with figure 5(g). The results in figure 6 demonstrate that diffraction losses cannot be neglected over distances comparable with the Rayleigh length, because dynamic confinement does not take place, as predicted. At variance
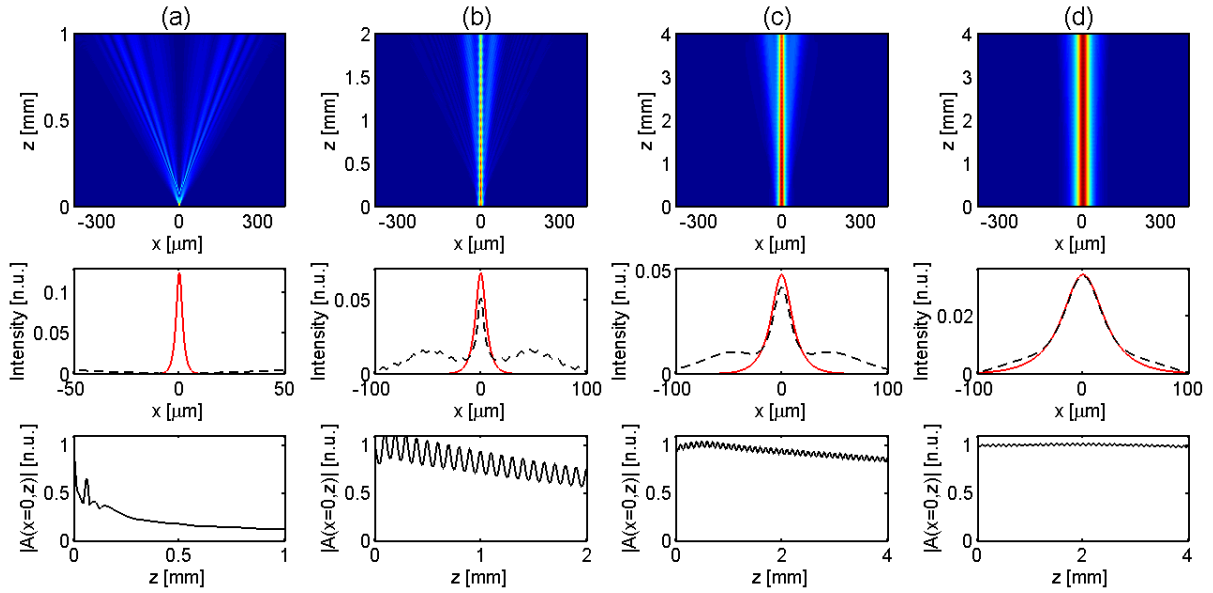
Figure 6. Intensity evolution in the plane xz (top) and corresponding profile at the input section $z = 0$ (solid red line, solution of (16)) and at the output (black dashed line) (middle); the bottom panels show the field amplitude in $x = 0$ versus z, normalized with respect to the initial value in $z = 0$. The trap width w_U is 3 (a), 10 (b), 20 (c) and 40 μm (d), respectively. Here $\lambda = 1\,\mu$m, $\Lambda = 100\,\mu$m and $U_0 = 0.05$.

with the solutions of equation (5), the light dynamics depends on w_U, as indicated by the fact that $L_{damp}w_U^{-2}$ is no longer conserved. The trend of the wavepacket peak versus z for the narrowest trap (column a, $w_U = 3\,\mu$m) differs qualitatively from the ones (columns b–d) computed for wider traps. For large w_U the intensity distribution can be normalized with respect to $z_{norm} = z/w_U^2$, analogously to equation (5), as the Rayleigh length is much shorter than the period Λ. The ratio between the Rayleigh length and Λ governs the longitudinal oscillations in the field peak, as well.

The strong dependence from w_U is in agreement with the physical mechanism behind the Kapitza effect: if diffraction is too strong (small w_U), the light can no longer be confined after a defocusing section. Mathematically, the spectrum of ϕ is large enough to induce aliasing; therefore equation (5) is not valid anymore, i.e. condition (4) is broken.

From the results above, it is straightforward to determine when light guiding via the Kapitza effect can occur and, if so, its dependence on w_U. To this extent, figure 7 plots the existence curves for the quasi-modes computed from equation (16), allowing us to pinpoint pairs of parameters Λ and w_U that allow Kapitza light confinement. The dashed line is the upper bound of the validity region for equation (16), as demonstrated by the results in figure 5. We have to apply equation (4) to assess when the simplified equation (5) is a good approximation for the original problem (1). In the plane of figure 7, condition (4) reads $w_{mode}/w_U > \Lambda/(\pi w_U)$: light confinement can occur in the region above the line starting from the origin and ending on the straight line $w_{mode}/w_U = 0.5$, with slope depending on the trap width w_U. Dynamic confinement is expected to occur in a triangular region, polygons ABC or ADC for w_{U1} or w_{U2}, respectively (see figure 7). Wider index wells provide a larger parameter region where
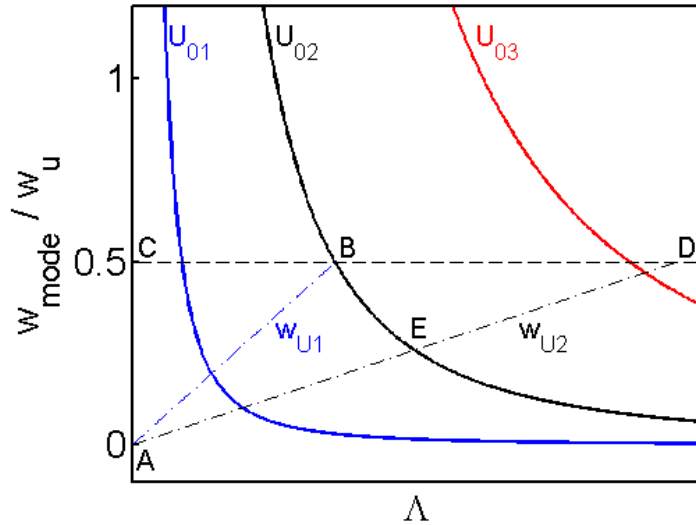
Figure 7. Qualitative assessment of dynamic confinement. The solid lines are the existence curves in the plane $(\Lambda, w_{\text{mode}}/w_U)$ as obtained from equation (16) for three index depths U_0, such that $U_{01} > U_{02} > U_{03}$. The dashed line representing $w_{\text{mode}}/w_U = 0.5$ is the upper bound of the validity region of the existence curves. The dashed-dotted lines represent the anti-aliasing condition (4) for two trap widths $w_{U1} < w_{U2}$, respectively.

dynamic confinement can take place. Moreover, for a given amplitude U_0 of the index well, the range of Λ allowing dynamic confinement can be found by computing the intersection of the corresponding existence curve with the straight line $w_{\text{mode}}/w_U = 0.5$ (i.e. the smallest Λ ensuring confinement) and with the line segment representing condition (4) (i.e. the largest Λ yielding confinement without significant oscillations in radius). With reference to figure 7, let us take $U_0 = U_{02}$: for $w_U = w_{U1}$ confinement occurs only at point B, whereas for $w_U = w_{U2}$ the wavepacket gets trapped in all the points belonging to the arc BE.

To validate the approach, we simulated light propagation in a periodic index well while varying the periodicity of $f(z)$, as well as the width and the peak value of $U(x)$. Typical results are presented in figure 8. For $w_U = 10\,\mu$m (upper panels) low loss dynamic confinement is never achieved for a trap depth U_0 up to 0.5. In fact, for short periods (figures 8(a) and (c)) the modal width overcomes $w_U/2$ (figure 7); thus the field tails couple energy toward the outer regions. For larger periods (figures 8(b), (d) and (e)) condition (4) is not valid: wherever the local index well is defocusing light diffracts outward, forming complicated patterns in (x, z) and diffusing photons across x. For $w_U = 40\,\mu$m diffraction is reduced and light confinement via the Kapitza effect takes place for all the used parameters (figures 8(f)–(j)). We note that for $U_0 = 0.1$, $\Lambda = 50\,\mu$m (figure 8(a)) and for $U_0 = 0.5$, $\Lambda = 10\,\mu$m (figure 8(c)) the quasi-mode retains nearly perfectly its shape over several Rayleigh lengths, that is, diffraction losses are negligible. When the period increases, aliasing comes into play, distorting the modal profile and generating oscillations in transverse size. Such oscillations are stronger for larger Λ due to the shift (in parameter space $(w_{\text{mode}}/w_U, \Lambda)$) toward the instability region (figure 7), eventually losing confinement, with dynamics analogous to the case $w_U = 10\,\mu$m previously discussed.
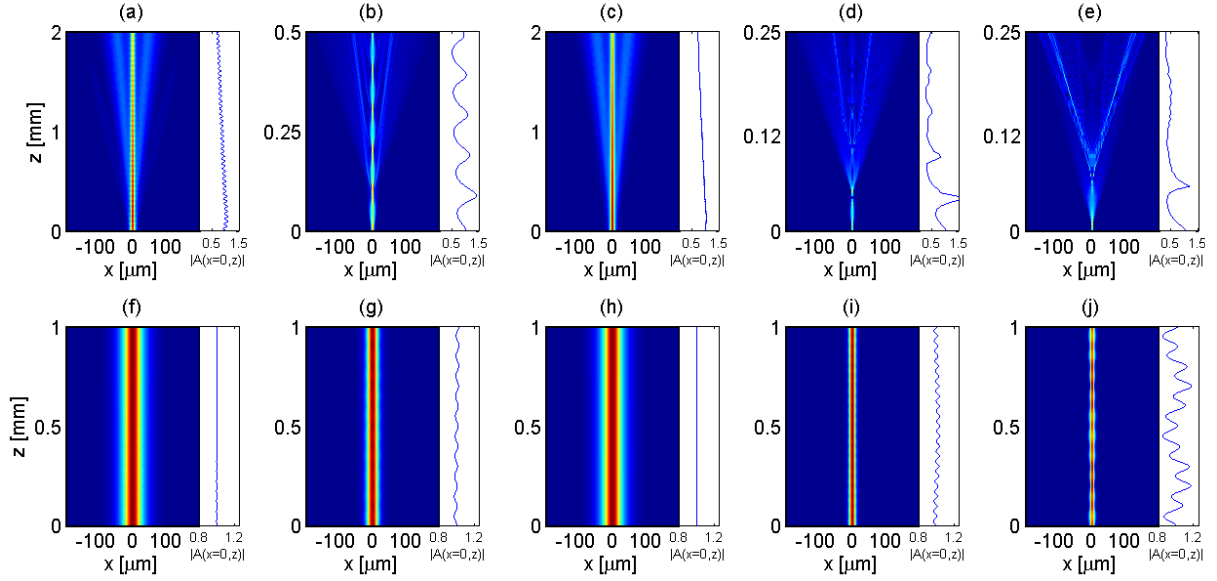
Figure 8. Intensity evolution in the plane xz (images) and behavior of the peak $|A(x = 0, z)|/|A(x = 0, z = 0)|$ versus z (panels next to each image) when a quasi-mode from equation (16) is launched at the input. Light propagation is calculated for $U_0 = 0.1$, $\Lambda = 50\,\mu$m (a), (f), $U_0 = 0.1$, $\Lambda = 100\,\mu$m (b), (g), $U_0 = 0.5$, $\Lambda = 10\,\mu$m (c), (h), $U_0 = 0.5$, $\Lambda = 50\,\mu$m (d), (i), $U_0 = 0.5$, $\Lambda = 100\,\mu$m (e), (j) and $w_U = 10\,\mu$m (a)–(e) and $w_U = 40\,\mu$m (f)–(j), respectively. Here $\lambda = 1\,\mu$m.

Table 1. Calculated $\overline{\Lambda}$ for various waveguide parameters.

U_0	w_U (μm)				
	10	20	30	40	50
0.1	38	51	62	72	81
0.5	16	24	31	37	43

To end this section, we assess the correctness of equation (4) resorting to BPM simulations. We define the period $\overline{\Lambda}(w_U, U_0) = \pi w_{\text{mode}}$, i.e. the value of Λ satisfying equation (4). In physical terms, $\overline{\Lambda}$ is the largest period ensuring dynamic light trapping when both w_U and U_0 are kept fixed; thus, in agreement with equation (6), at $\overline{\Lambda}$ light trapping is the strongest. In addition, we conveniently define $\overline{\Lambda}_{\text{sup}}(w_U)$ as the maximum of $\overline{\Lambda}$ for a fixed trap width w_u, with the extra constraint $w_{\text{mode}} \leqslant 0.5 w_U$ (in figure 7 such a point for w_{U1} is indicated by B). The use of equation (4) easily provides $\overline{\Lambda}_{\text{sup}} = \frac{\pi}{2} w_U$. A direct comparison between $\overline{\Lambda}$ and $\overline{\Lambda}_{\text{sup}}$ indicates whether the dynamic effect can be achieved for the given pair (U_0, w_U): if $\overline{\Lambda} > \overline{\Lambda}_{\text{sup}}$ Kapitza-like confinement is inhibited by diffraction losses, if $\overline{\Lambda} < \overline{\Lambda}_{\text{sup}}$ light trapping can occur.

Table 1 is obtained from the data in figure 4. For $w_U = 10$ and $40\,\mu$m, we get $\overline{\Lambda}_{\text{sup}} \approx 16$ and $63\,\mu$m, respectively. The theoretical predictions can be compared with the full numerical simulations in figure 8. We start with the case $w_U = 10\,\mu$m. For $U_0 = 0.1$ (figures 8(a) and (b))

light is not confined, consistently with table 1. For $U_0 = 0.5$ there are small diffraction losses for $\Lambda \approx \overline{\Lambda}_{\mathrm{sup}} = 16\,\mu\mathrm{m}$ (figure 8(c)): the confinement is borderline as this is the limit condition $\overline{\Lambda} = \overline{\Lambda}_{\mathrm{sup}}$ (corresponding to point B in figure 7), where both a strong overlap of the mode with the edges of the effective index well and aliasing are simultaneously present. Due to the joint action of the two detrimental effects, the best light localization is reached for $\Lambda \approx 20\,\mu\mathrm{m} \neq \overline{\Lambda}_{\mathrm{sup}}$. We now turn to the case $w_U = 40\,\mu\mathrm{m}$: looking up table 1, light should not be guided for $U_0 = 0.1$; in spite of this, figures 8(f) and (g) show a collimated wavepacket thanks to the large L_{damp} compared with the Rayleigh length. For $U_0 = 0.5$ light confinement should occur, as confirmed by figures 8(h) and (i): further numerical simulations (not shown) prove that the narrowest quasi-mode, jointly with the smallest oscillations in radius, is excited for $\Lambda \approx 35\,\mu\mathrm{m}$, in perfect agreement with the theoretical predictions. The numerical results also demonstrate that transverse confinement occurs even for $\Lambda > \overline{\Lambda}$, but with the quasi-mode undergoing appreciable periodic variations of its width (see figures 8(i) and (j)). The existence of trapped breathing waves for $\Lambda > \overline{\Lambda}$ agrees with our theory: smooth transition in the character of light propagation can be expected when condition (4) is slightly missed, the latter corresponding to weakly overlapping replicas of $\tilde{\phi}$.

4.1. Dependence on the index profile $U(x)$

Up to now in our simulations we have considered a Gaussian $U(x)$, but light trapping via the Kapitza effect can be assessed for various $U(x)$ using figure 7. A non-Gaussian $U(x)$ implies different existence curves for the quasi-modes and different diffraction losses α for a given modal width as well; the latter modify the applicability range of equation (16), rewritten for the new $U(x)$. Furthermore, if the modal width is fixed, a different $U(x)$ affects the profile u of the quasi-mode, with small changes in condition (4); considering the numerical results discussed in section 4, the latter changes are expected to be negligible.

In section 3, we calculated the effective index well for a super-Gaussian $U(x)$ (see equation (15)), as this ansatz permits us to address the role of the abruptness of $U(x)$ in the efficiency of dynamic confinement. Substitution of equation (15) into equation (5) demonstrates that, in complete analogy with the Gaussian case $p = 1$, for every value of p light propagation depends on the normalized transverse (longitudinal) coordinate x/w_U ($z_{\mathrm{norm}} = z/w_U^2$). Figure 9(a) shows sample solutions u of the equivalent of equation (16) as p varies, for fixed Λ and U_0. When p is small, the optical modes resemble a Gaussian function, whereas for large p they are similar to sinusoidal branches, as in slab waveguides. The latter is confirmed by figure 9(b) showing the degree of confinement versus Λ. In fact, when the modal width w_{mode} is smaller than w_U (i.e. for large Λ), trapping improves when p is smaller due to shrinking of the region with a flat Δn_{eff}. In the opposite limit of modal widths comparable with w_U, light confinement improves with p owing to sharper peaks near the edges of Δn_{eff} (from equation (15) the peak of the effective index well is roughly proportional to p^2). This interpretation of the p dependence for dynamic light trapping fully accounts for the behavior of Δn_{eff} in figure 9(c), as well. Figure 9(d) graphs the diffraction losses associated with the quasi-modes: for a fixed p the coefficient α has the same qualitative behavior of the Gaussian case $p = 1$, with α diminishing for larger p.

The degree of confinement of the modes computed in figure 9 was also investigated via BPM, as shown in figure 10. As p increases, the maximum Λ ensuring trapping becomes larger (see the amplitude peak versus z in figures 10(a)–(d)): in fact, the higher the p, the flatter the
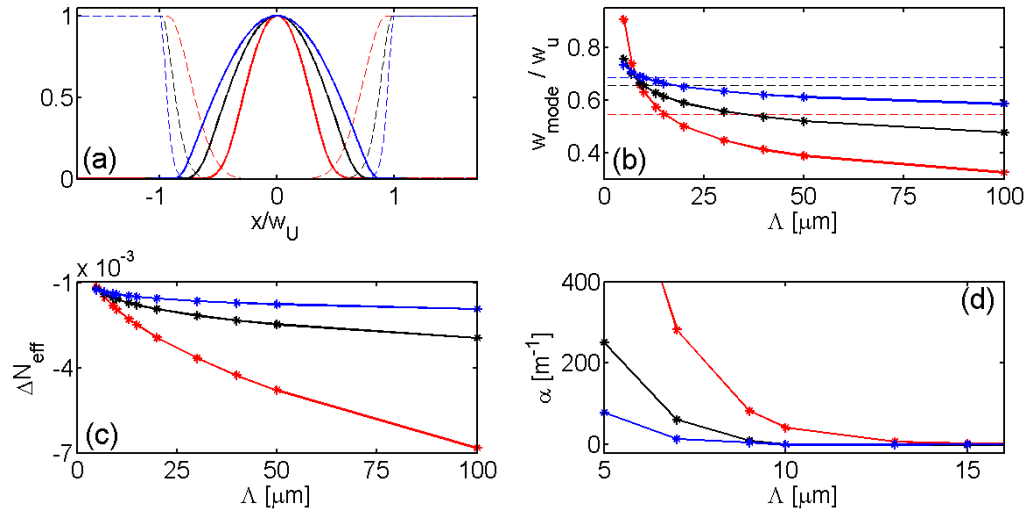
Figure 9. (a) Quasi-mode profiles u versus x/w_U for $\Lambda = 100\,\mu\text{m}$ and $p = 2$ (red solid line, narrowest profile), $p = 4$ (black solid line, intermediate width) and $p = 8$ (blue solid line, widest profile); the dashed lines are inverted replicas of the index wells with depth normalized to 1. (b) Normalized width of the quasi-mode w_{mode}/w_U, (c) changes in effective index ΔN_{eff} and (d) diffraction losses α versus period Λ for $p = 2$ (red line with symbols), $p = 4$ (black line with symbols) and $p = 8$ (blue line with symbols); the dashed lines correspond to the widest quasi-mode with negligible losses for a fixed p. In (d) the loss coefficient was calculated for $w_U = 5\,\mu\text{m}$. Here $U_0 = 0.5$ and $\lambda = 1\,\mu\text{m}$ in all the simulations.

existence curve of the modes for large Λ (see figure 9(b)). At the same time, the oscillations along z get bigger with p, even for $\Lambda = \overline{\Lambda}$, the latter ascribable to a larger spectrum $\tilde{\phi}$ for a given width. Moreover, even if the average peak appears nearly unaltered along z, small losses occur in the defocusing regions. The presence of radiated light can be inferred from the calculated width of the wavepacket along z (figures 10(e)–(h)), with radiation increasing with p, as well. Finally, figures 10(i)–(l) display the computed intensity evolution in the plane xz for $p = 8$ and four Λ. Despite the stronger diffraction losses with respect to the Gaussian case $p = 1$, light is still confined for Λ up to $3\overline{\Lambda}_{\text{sup}}$, i.e. the Kapitza effect is effective on a larger interval of Λ.

4.2. Dependence on longitudinal modulation $f(z)$

After investigating the role of the transverse profile $U(x)$ on dynamic confinement, we study how the Kapitza effect depends on the modulation $f(z)$ for a given periodicity. Equation (6) states that, once $U(x)$ is fixed, the transverse profile of the confining potential does not change with $f(z)$, the latter acting on the amplitude of the effective well. In this section, we take a Gaussian $U(x)$ and consider various $f(z)$.

The comparison between different $f(z)$ has to be carried out for a fixed depth U_0, the latter imposed by technological limitations. Comparing, for example, equations (7) (sine modulation) and (8) for $d/\Lambda = 0.5$ (square wave) with U_0 kept constant, it is clear that the overall amplitude of Δn_{eff} for the square wave is about $16/\pi^2$ times larger than in the sinusoidal case. Thus, the
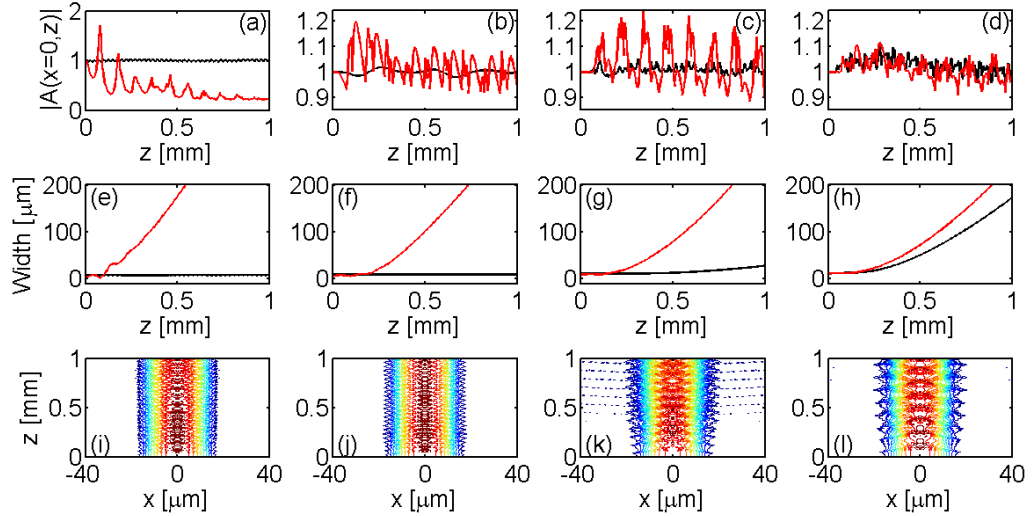
Figure 10. Upper and middle rows: normalized amplitude peak (a)–(d) and mode width (e)–(h) versus z for $p = 1$ (a), (e), $p = 2$ (b), (f), $p = 4$ (c), (g) and $p = 8$ (d), (h), respectively; black and red lines correspond to $\Lambda = \overline{\Lambda}$ and $3\overline{\Lambda}_{\text{sup}}$, respectively (for the chosen parameters $\overline{\Lambda} < \overline{\Lambda}_{\text{sup}}$ is valid). Bottom: contour plots of light intensity evolution in the plane xz for $p = 8$ and period Λ equal to $\overline{\Lambda}$ (i), $\overline{\Lambda}_{\text{sup}}$ (j), $2\overline{\Lambda}_{\text{sup}}$ (k) and $3\overline{\Lambda}_{\text{sup}}$ (l), respectively. Here $w_U = 20\,\mu\text{m}$, $U_0 = 0.5$ and $\lambda = 1\,\mu\text{m}$.

quasi-modes are exactly the same if we compare the square wave with $U_0 = U'$ with a sine wave featuring $U_0 = (4/\pi)U'$. Analogous considerations are valid for flat-top modulations when the role played by the duty cycle d/Λ has to be accounted for (see figure 1(b)). BPM simulations (not shown) indicate that when wavepackets undergo transverse confinement, identical quasi-modes at the input evolve in a similar manner along z, regardless of the shape of $f(z)$.

To confirm the statements above, we performed numerical simulations as summarized in figure 11 for various modulations $f(z)$, keeping $U(x)$ constant. From the direct comparison of figures 11(a)–(c) with figures 11(d)–(f), the dynamics of light propagation with period Λ (see figure 10) indicates a lower Δn_{eff} for the sine case than for the square wave case (note that in figure 11(f) the wavepacket breaks up due to the outstanding narrowness of the quasi-mode). The comparison between the middle and bottom panels is consistent with the results in figure 1(b), that is, for $d/\Lambda = 0.1$ the effective index well is weaker than for $d/\Lambda = 0.5$. For $d/\Lambda = 0.1$ the wavepacket undergoes appreciable diffraction losses for $\Lambda = 30\,\mu\text{m}$ (figure 11(g)), whereas for $\Lambda = 90\,\mu\text{m}$ it is still trapped (figure 11(i)) because condition (4) is satisfied, at variance with figure 11(f).

4.3. Dependence on input section

As pointed out in section 2.1, the phase fronts of the quasi-modes found via equation (16) exhibit a periodic curvature versus z (see equation (2)), i.e. the transverse phase is constant only in specific sections $z = \text{const}$. Otherwise stated, a periodic guide, unlike standard (longitudinally uniform) structures ensuring *static* confinement, does not possess longitudinal invariance with

IOP Institute of Physics **Φ** DEUTSCHE PHYSIKALISCHE GESELLSCHAFT
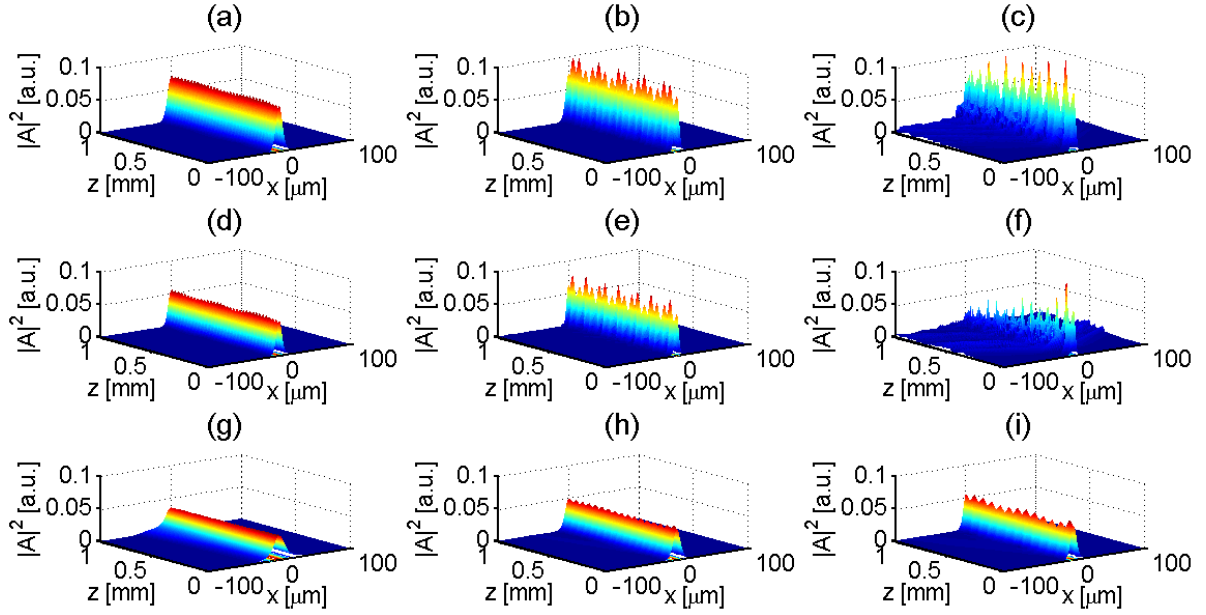
Figure 11. Comparison between different longitudinal modulations $f(z)$. Intensity evolution for sinusoidal $f(z)$ (a)–(c), for flat-top $f(z)$ with $d/\Lambda = 0.5$ (d)–(f) and $d/\Lambda = 0.1$ (g)–(i), respectively. The period Λ is either $30\,\mu$m (a), (d), (g) or $60\,\mu$m (b), (e), (h) or $90\,\mu$m (c), (f), (i), respectively. Here $w_U = 20\,\mu$m, $U_0 = 0.5$ and $\lambda = 1\,\mu$m.
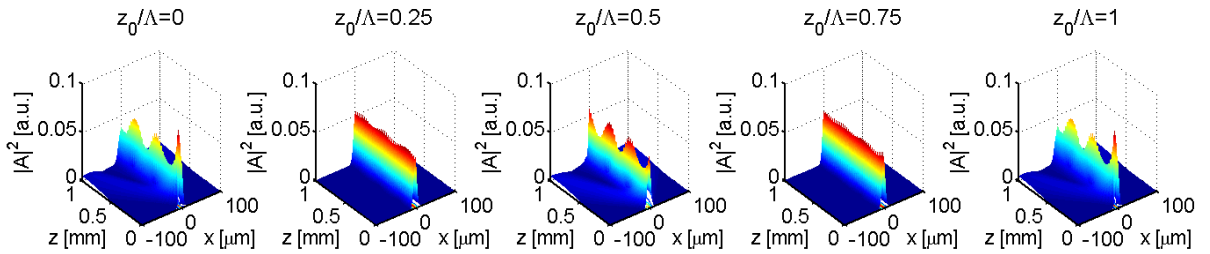
Figure 12. Light propagation for a quasi-mode launched at different z_0. Here $w_U = 20\,\mu$m, $\Lambda = 30\,\mu$m, $d/\Lambda = 0.3$, $U_0 = 0.5$ and $\lambda = 1\,\mu$m.

respect to z; hence, in order to minimize coupling/insertion losses, the quasi-mode computed via equation (16) needs be launched in specific z_0, the latter depending on the form of the periodic $f(z)$. For flat-top modulation, we previously demonstrated that equation (9) is valid; hereby we test the theoretical prediction by means of BPM simulations. The numerical results for flat-top modulation with $d/\Lambda = 0.3$ are visible in figure 12. As predicted by equation (9), optimum input coupling is achieved for $z_0 = 0.25\Lambda$ and 0.75Λ. For the other values of z_0 the diffraction losses are apparent, together with an appreciable breathing of the modal profile versus z. Additional simulations (not shown here) for different ratios d/Λ as well as in the sinusoidal case validate our theoretical approach.
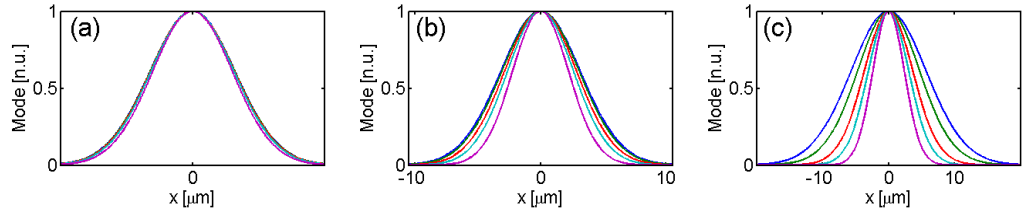
Figure 13. Modal profiles, normalized to their peak, computed via equation (18) for $\gamma = 1$ (a), 0.1 (b) and 0.01 (c), respectively. Each line corresponds to a period Λ, given by 1, 20, 40, 60 and 100 μm, from widest to narrowest profiles, respectively. We note that in the case $\Lambda = 1\,\mu$m the Kapitza effect is almost uninfluent.

5. Interplay of dynamic and static confinement

So far we assumed no static confinement, as we considered periodic index distributions with a net zero average contrast. In this section we study the interplay between static and dynamic confinement in unbalanced z-periodic structures. To this extent, in equation (1) we take a refractive index of the form

$$\Delta n(x, z) = \big[\gamma + f(z)\big] U(x), \tag{17}$$

where the average of $f(z)$ is still zero. The real coefficient γ weighs static versus dynamic index wells. We stress that equation (17) is not the most general, as we assume the same transverse profile $(U(x))$ for both the static and the periodic components of Δn; nevertheless, this does not hamper the general conclusions while it models realistic geometries (e.g. segmented waveguides [13–16]).

By looking at equations (2) and (3), it appears that a static component is equivalent to introducing in equation (3) new terms proportional to z, thus rendering inappropriate the approach used for $\overline{f} = 0$. We can argue that a static (cw) component introduces an extra phase modulation across x, which in turn adds to the phase stemming from the Kapitza effect, until the cw portion of Δn appreciably modifies the field profile over a single period Λ. Mathematically, we compute the modes of the structure via

$$2k_0 n_0 \Delta\beta_{\text{eff}} u = \frac{\partial^2 u}{\partial x^2} + k_0^2 \big[2\gamma n_0 U(x) + \Delta n_{\text{eff}}(x)\big] u \tag{18}$$

with Δn_{eff} still expressed by equation (6). Hereafter, for conciseness we set $U(x)$ Gaussian with $U_0 = 0.5$ and $w_U = 20\,\mu$m, and $f(z)$ sinusoidal; thus, equation (15) for $p = 1$ describing the effective dynamic potential due to the Kapitza effect is valid.

Figure 13 displays the numerical solutions of (18) for three values of γ. When $\gamma = 1$, the cw and the periodic components have the same amplitude; thus the index contrast never goes negative, as in segmented waveguides: according to figure 13(a) the Kapitza effect does not affect the modal profile. Conversely, for lower γ (figures 13(b) and (c)) the Kapitza trapping becomes relevant: the modal profile u undergoes appreciable variations as the period Λ changes; in particular it shrinks for large Λ in agreement with equation (6).

Next we analyze the shape and stability of the modes using BPM simulations. We start with the case $\gamma \ll 1$, i.e. when the dynamic phase is relevant according to figure 14. We choose $\gamma = 0.01$ to maximize the dynamic effects. Since the quasi-modes supported by the Kapitza
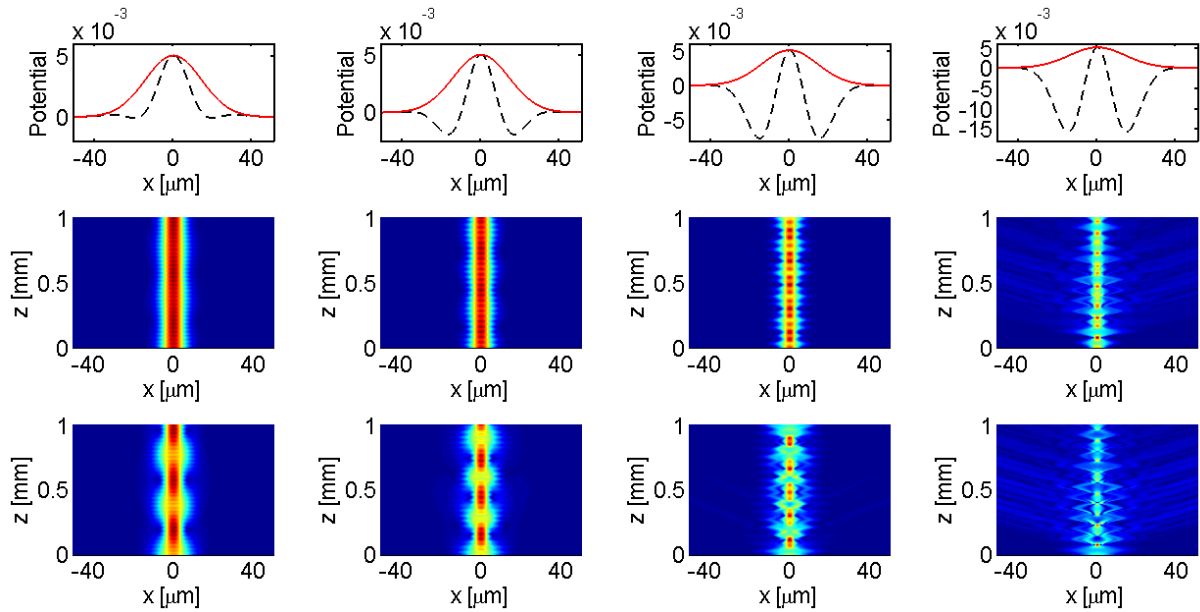
Figure 14. Top row: static (red solid line) and complete (static plus dynamic effects, dashed black line) potential versus x for $\gamma = 0.01$. Middle row: intensity evolution in the plane xz when the input field is a solution of equation (18) for $\gamma = 0.01$. Bottom: as in the middle but the mode from equation (18) is computed neglecting the Kapitza effect. From left to right, Λ is 30, 40, 60 and 80 μm, respectively. Here $w_U = 20\,\mu$m, $U_0 = 0.5$ and $\lambda = 1\,\mu$m.
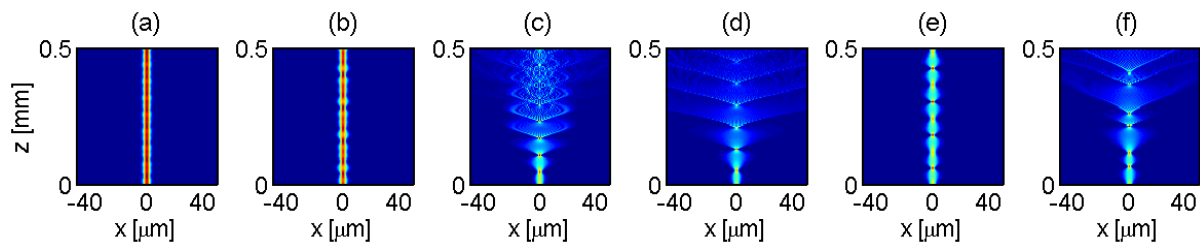
Figure 15. Propagation of quasi-modes for $\gamma = 1$. The periods Λ are 30 (a), 40 (b), 60 (c), 80 (d), 120 (e) and 150 μm (f), respectively.

effect are not perfectly invariant along z, but undergo oscillations and eventually break up for large Λ (see figure 8), we compare their evolution when the dynamic phase is included (middle row in figure 14) and when it is neglected (bottom row in figure 14). The results show clearly that modes are more localized when the Kapitza effect is accounted for, demonstrating the validity of equation (18). As we found for $\gamma = 0$ (see figure 11), no localization occurs for large Λ as condition (4) is not satisfied.

We now examine the case $\gamma = 1$. The modes are slightly affected by the Kapitza effect (figure 13(a)), but we need to check whether they break up for large Λ, as occurs for small or vanishing γ. Figure 15 shows the typical behavior for various periods Λ. For small Λ, the periodic modulation induces only small oscillations along z; for large enough Λ, diffraction

in the low index regions is no longer compensated by focusing in the high index regions, resulting in strong coupling to radiation. Noteworthy, for even larger Λ the wavepacket acquires once again a localized structure, even if undergoing strong oscillations along z due to the simultaneous excitation of several modes. Further increases in period yield loss of confinement. This is not observed for small γ and can be ascribed to resonance effects between multimodal interference in the guide and longitudinal modulation of refractive index.

6. Conclusions

We have discussed light propagation in guided-wave dielectric structures subject to a periodic longitudinal modulation of the refractive index distribution. While existing models of segmented waveguides state that light propagates according to an average index well along z, yielding no confinement for a vanishing average index contrast, we found that confinement can take place even in the balanced case owing to a transverse modulation of the wavevector, similarly to the Kapitza effect in quantum mechanics. Using BPM simulations we discussed light propagation versus geometric parameters, including the profile of the index well versus x and the form of the longitudinal modulation along z. We introduced a graphic method to roughly estimate light trapping and its range of validity within the Kapitza model. In particular, wide wavepackets are not confined due to strong coupling with diffractive losses to radiation, whereas very narrow modes break up due to aliasing phenomena. Remarkably enough, several concepts stemming from our analysis in optics also apply to quantum mechanics where, to the best of our knowledge, they are a novelty.

Although the experimental observation and demonstration of the proposed new mechanism for light trapping might be a challenge (particularly in anisotropic dielectrics), table 1 indicates that dynamic confinement can be accessed for index changes in the range ± 0.1–0.5 in transverse regions of tens of micrometers. These levels of index contrast could be obtained in semiconductor heterostructures (e.g. AlGaAs composites [28]), in voltage biased electro-optic crystals or liquid crystals [29]. In the latter, the refractive index profile could be easily controlled—both transversely and longitudinally—by applying external electric fields or defining non-uniform boundary conditions [30–33]. The required periods of the longitudinal modulation are well within those achievable with lithographic techniques. Finally, we studied the interplay between dynamic confinement (due to the periodic modulation of the index) and static confinement (due to a cw index contrast), analyzing the role of their mutual interplay versus waveguide parameters.

We believe our findings pave the way to a new family of optical waveguides and photonic devices with exotic features and large tunability; moreover, these results can trigger the investigation of chaos in wave mechanics. The generalization to nonlinear cases can unveil new kinds of solitons and solitary waves based on the Kapitza effect.

Acknowledgments

IOP Institute of Physics ⬥ DEUTSCHE PHYSIKALISCHE GESELLSCHAFT

References

[1] Elachi C and Yeh C 1973 *J. Appl. Phys.* **44** 3146–52
[2] Bierlein J D, Laubacher D B, Brown J B and van der Poel C J 1990 *Appl. Phys. Lett.* **56** 1725–7
[3] Suhara T and Nishihara H 1990 *IEEE J. Quantum Electron.* **26** 1265–76
[4] Yariv A 1997 *Optical Electronics in Modern Communications* (Oxford: Oxford University Press)
[5] McLeod H A 2001 *Thin-Film Optical Filters* (London: CRC)
[6] Eisenberg H S, Silberberg Y, Morandotti R and Aitchison J S 2000 *Phys. Rev. Lett.* **85** 1863–6
[7] Yablonovitch E, Gmitter T J and Leung K M 1991 *Phys. Rev. Lett.* **67** 2295–8
[8] Longhi S and Staliunas K 2008 *Opt. Commun.* **281** 4343–7
[9] Cuevas J, Malomed B A and Kevrekidis P G 2005 *Phys. Rev.* E **71** 066614
[10] Assanto G, Minzoni A A, Ben S, Smyth N F and Worthy A L 2010 *Phys. Rev. Lett.* **104** 053903
[11] Szameit A, Kartashov Y V, Dreisow F, Heinrich M, Pertsch T, Nolte S, Tünnermann A, Vysloukh V A, Lederer F and Torner L 2009 *Phys. Rev. Lett.* **102** 153901
[12] Joushaghani A, Iyer R, Poon J K S, Aitchison J S, de Sterke C M, Wan J and Dignam M M 2009 *Phys. Rev. Lett.* **103** 143903
[13] Li L and Burke J J 1992 *Opt. Lett.* **17** 1195–7
[14] Nir D, Weissman Z, Ruschin S and Hardy A 1994 *Opt. Lett.* **19** 1732–4
[15] Ortega D, Aldariz J M, Arnold J and Aitchison J S 1999 *J. Lightwave Technol.* **17** 369–75
[16] Hochberg M, Baehr-Jones T, Walker C, Witzens J, Gunn L C and Scherer A 2005 *J. Opt. Soc. Am.* B **22** 1493–7
[17] Weissman Z and Hardy A 1993 *J. Lightwave Technol.* **11** 1831–8
[18] Cook R J, Shankland D G and Wells A L 1985 *Phys. Rev.* A **31** 564–7
[19] Kapitza P L 1951 *Zh. Eksp. Teor. Fiz.* **21** 588–97
[20] Paul W 1990 *Rev. Mod. Phys.* **62** 531–40
[21] Longhi S 2009 *Laser Photon. Rev.* **3** 243–61
[22] Rahav S, Gilary I and Fishman S 2003 *Phys. Rev. Lett.* **91** 110404
[23] Longhi S 2011 *Opt. Lett.* **36** 819–21
[24] Rizza C and Ciattoni A 2013 *Phys. Rev. Lett.* **110** 143901
[25] Ridinger A and Davidson N 2007 *Phys. Rev.* A **76** 013421
[26] Landau L D and Lifshitz E M 1976 *Course in Theoretical Physics Mechanics* (Oxford: Pergamon)
[27] Hu J and Menyuk C R 2009 *Adv. Opt. Photon.* **1** 58–106
[28] Aspnes D E, Kelso S M, Logan R A and Bhat R 1986 *J. Appl. Phys.* **60** 754–67
[29] Khoo I C 1995 *Liquid Crystals: Physical Properties and Nonlinear Optical Phenomena* (New York: Wiley)
[30] Residori S 2005 *Phys. Rep.* **416** 201–72
[31] Gilardi G, Asquini R, d'Alessandro A and Assanto G 2010 *Opt. Express* **18** 11524–9
[32] Slussarenko S, Murauski A, Du T, Chigrinov V, Marrucci L and Santamato E 2011 *Opt. Express* **19** 4085–90
[33] Barboza R, Alberucci A and Assanto G 2011 *Opt. Lett.* **36** 2725–7